Internal wettability investigation of mesoporous silica materials by ellipsometric porosimetry

Máté Füredi[1,2], Bálint Fodor[2,*], András Marton[2], Alberto Alvarez-Fernandez[1,3], Aysha A Riaz[4], Curran Kalha[4], Anna Regoutz[4], Stefan Guldin[1], Péter Basa[2]

[1]*Department of Chemical Engineering, University College London, Torrington Place, London, WC1E 7JE, UK*

[2] *Semilab Co. Ltd., Prielle Kornélia u. 4/A. H-1117 Budapest, Hungary*

[3]*AMBER Research Centre, School of Chemistry, Trinity College Dublin, Dublin, Ireland*

[4]*Department of Chemistry, University College London, 20 Gordon Street, London WC1H 0AJ, UK*

*E-mail address: balint.fodor@semilab.hu

Abstract

Silica-based mesoporous films have been widely applied in the fabrication of advanced functional materials, such as anti-reflective coatings, bio-, and chemical sensing devices, due to their unique properties, e.g., high surface area, controlled porosity, and the ease and tailorability of their synthesis. Precise knowledge of their pore architecture is crucial, highlighting the need for accurate characterization tools. In this sense, ellipsometric porosimetry represents a powerful and versatile characterization platform, providing access to reliable information about total porosity, pore size, pore size dispersity, mechanical properties (Young's modulus) and surface area of a great variety of mesoporous thin films.

While the underlying framework of modelling capillary condensation via the Kelvin equation is well established, one descriptor, the internal wettability of mesoporous architectures remains a challenging variable for reliable material characterization. Wetting on the nanoscale cannot be observed via the traditional drop-shape method, while approximating internal wetting by the macroscopic property can be inaccurate as the two wetting behaviors do not necessarily correlate. Herein, we present a method based on vacuum ellipsometric porosimetry for the determination of the internal contact angle of functionalized mesoporous silica thin films. Tuning of the surface energy for a known mesoporous architecture by methyl-functionalization enabled us to relate differences in the pore filling for various adsorptives (water, methanol, toluene, cyclohexane) to their internal contact angles. Our study serves as a guide for generalized internal contact angle determination suitable for a wide range of organic adsorptives and mesoporous sorbent

materials.

1. Introduction

Wettability of nanostructured surfaces is a key property to consider in all applications where liquid-solid interfaces play a crucial role, such as functional coatings [1], smart windows [2], membranes [3], gas-sensing devices [4,5], and nano-based drug delivery systems [6]. However, while the investigation of wettability and the determination of contact angle (θ) is routinely performed on planar surfaces with simple experimental setups, the thus-acquired macroscopic wettability does not necessarily correspond to the intrinsic (microscopic) wetting behavior of nanostructured materials [7,8].

In the last two decades, ellipsometric porosimetry (EP) has become one of the most powerful characterization techniques for mesoporous thin films, providing reliable porosity, pore size, specific surface area, and Young's modulus information in a purely optical, non-destructive way for thin film mono-, and multilayers [9–13]. As a porosimetric measurement, EP relies on the manipulation of the relative pressure of an adsorptive (in most cases water, toluene, or 2-propanol), while the mesopore filling is monitored via spectroscopic ellipsometry (SE) measurements. Using optical models with effective medium approximations (EMA), the volume of liquid adsorbed relative to the total sorbent volume (V_{ads}/V_{tot}) can then be calculated at each relative pressure step, enabling the construction of adsorption/desorption volume isotherms. As neither absolute volumetric nor gravimetric measurements are necessary for pore filling calculations, the accuracy of the measurements is not affected by total sample mass, making the method more reliable for the measurement of thin films compared to traditional powder-based porosimetry techniques, such as nitrogen physisorption with Brunauer–Emmett–Teller analysis [14].

Pore size distribution (PSD) data can be obtained from the volume adsorbed isotherm based on the relationship between mesopore size and capillary condensation described by the Kelvin-equation. For more accurate PSD calculations the modified Kelvin-equation (eq. 1) which also accounts for the statistical monolayer formation [9,15,16] during the adsorption process can be written as

$$\ln\left(\frac{P}{P_0}\right) = \frac{-2V_m * \gamma * \cos\theta_i}{R*T\left(\frac{D_{pore}}{2} - t_c\right)} \tag{1}$$

where P/P_0 is the relative pressure V_m and γ are the molar volume and surface tension of the adsorptive liquid respectively, θ_i is the internal contact angle, R is the universal gas

constant, T is the absolute temperature, D_{pore} is the pore diameter, and t_c is the monolayer correction parameter. One source of inaccuracy in the usage of the modified Kelvin-equation remains the internal contact angle parameter (θ_i). While most works have assumed this to be 0° [17,18] or substituted it with the macroscopic contact angle [19], this may not always be a correct approximation [8]. For obtaining more realistic θ_i values, Baklanov et al. introduced a simple estimation of water wettability inside low-k type porous material with EP by simply comparing water and toluene adsorption [20]. The aim of our work is two-fold. On one hand, we are extending EP-based internal wetting characterization beyond water with the use of vacuum EP and organic adsorptives, in order to obtain accurate PSD information for surfaces with $\theta_i > 0°$ [8,21,22]. On the other hand, by investigating multiple adsorptives ranging from highly polar to nonpolar (water, methanol, toluene, and cyclohexane) on a series of functionalized silica surfaces, we are presenting a powerful method for systematically comparing the internal wettability of a materials library with a wide range of surface energies towards liquids with a broad spectrum of polarities.

2. Experimental

2.1 Sample preparations

1.5 g Tetraethyl-orthosilicate (Sigma >99%) was mixed with 0.788 ml ethanol (Sigma, 99.8%), with the subsequent dropwise addition of 0.746 ml 10 mM hydrochloric acid (ACS reagent, 37%, Merck). The thus-prepared sol was stirred at room temperature for 3 hours before pipetting and transferring 0.360 ml to a new vial and mixing with 11.6 m/m% ethanolic solution of poly(ethylene oxide)-block-poly(propylene oxide)-block-poly(ethylene oxide), PEO_{106}-PPO_{70}-PEO_{106} (PF127, from Sigma) to reach 1:0.005 TEOS:PF127 molar ratio. The mixture was then spin-coated (using a Laurell WS-650-23NPPB spin-coater) at 5000 rpm onto 2x2 cm silicon wafer cuts. To remove the block copolymer template, the samples were calcined in a muffle furnace at 450 °C for 30 mins (5°C /min ramping speed). After cooling down, thin films were activated in a Diener Femto oxygen plasma etcher for 300 s, then immediately placed in a freshly prepared room temperature 7 vol/vol% trimethylsilyl chloride (TMCS, >98% from Sigma)/n-hexane (Honeywell, >97%) mixture for functionalization. After a set amount of time has passed (varied between 30 mins to 5 hours) the samples were removed and thoroughly washed with n-hexane.

2.2 Sample Characterization

<u>Ellipsometric porosimetry:</u> Semilab PS-2000 rotating compensator spectroscopic ellipsometer with vacuum chamber for porosimetry measurements was used to obtain EP data with water (ultrapure, 18.2 MΩ·cm), methanol (a.r., 99,99%,), toluene (ACS reagent, 99,97%), and cyclohexane (for HPLC, 99,99%). All samples were heat cured at 150° C for 10 minutes before placing them in the vacuum chamber. The measurements were performed at an incidence angle of 60°. Volume adsorbed ratios and accessible porosities were calculated via the Lorentz-Lorenz EMA where only the refractive indices of the adsorbates have to be taken from reference values (the calculated volume ratios are independent of the refractive index of the silica skeleton matrix if a constant value is assumed during the EP cycle) [16]. Total porosity values were calculated independently of porosimetric measurements via two-component (SiO_2 and void) Lorentz-Lorenz EMA fitting of the initial SE spectra of the water adsorption experiment at the P/P_0=0 step (<7 Pa vacuum).

<u>X-ray photoelectron spectroscopy (XPS):</u> XPS measurements were performed using a

Thermo Scientific K-Alpha XPS spectrometer, equipped with a monochromated Al Kα (1.4867 keV) X-ray source, a 180° double focusing hemispherical analyser and a 128-channel detector. A different set of samples has been prepared using identical recipe for the measurements which have not undergone any EP cycles, and which were placed in the vacuum ch amber within 24 hours after the functionalization has finished. Samples were cut to a size of 1x1 cm^2 using a diamond tipped pen and fixed to a sample plate using adhesive conductive carbon tape. No additional ex-situ or in-situ sample preparation was carried out prior to the measurements. The spectrometer was operated under a base pressure of 3.3×10^{-6} Pa and an X-ray spot size of 400 μm was used for the collection of spectra. The Si 2p, C 1s, O 1s and F 1s core level spectra were collected along with a survey spectrum for all samples. During the acquisition of these spectra, a flood gun was used to mitigate against surface charging. The spectra were collected with a pass energy of 20 eV, a dwell time of 75 ms and a step size of 0.1 eV. The processing of the spectra, including elemental quantification, was performed using the Thermo Scientific Avantage v.5.9925 software package. All acquired core level spectra were normalised to the Si 2p peak area. The Smart background option as implemented in the Avantage software package was used for peak fit analysis, which is based on a Shirley type background function. A Voigt line shape was applied with both the Lorentzian/Gaussian ratio as well as the line width allowed to refine for all samples.

Fourier-transform infrared (FTIR) spectroscopy: FTIR spectra were recorded on a Perkin Elmer Frontier spectrometer using the attenuated total reflectance technique on different set of samples which have been prepared using identical recipe on gold evaporated (100 nm thickness) silicon substrates. Spectral data were collected in the mid-IR range (4000–500 cm^{-1}) with 16 scans and 4 cm^{-1} resolutions. A background spectrum (16 scans) was recorded before measuring each sample spectrum.

Macroscopic wettability: Macroscopic contact angles were captured using a Kruss DSA100 drop-shape analyzer. Test liquid droplets of ~5 µl were deposited on the studied surfaces and contact angle values were calculated from the shapes of the three-phase contact lines based on the average of two measurements.

3. Results and discussion

Functionalized SiO₂ mesoporous thin films were prepared following the micelle templating fabrication approach [23,24], as sketched in **Figure 1**. PF127, a tri-block copolymer (BCP) was used as structure-directing agent, which was previously shown to favor cubic arrangement of micelles in the used ratio [25]. In a first step, SiO₂ sol-gel precursors were embedded in the corona of the BCP micelles via preferential interactions (**Figure 1A**). In a subsequent step, the hybrid solution was cast on silicon substrates by spin coating **(Figure 1B)**. After calcination, the mesoporous structure was revealed (**Figure 1C**). Finally, the surface chemistry of the obtained mesoporous coating was modified by reaction with TMCS (**Figure 1D**), which has small enough molecular size to easily diffuse into mesopores [26]. The SE spectra of the prepared films could be fitted using a simple 1-layer Cauchy dispersion law with coefficients of determination over 0.998, indicating no significant roughness or thickness inhomogeneity within the measured spot. The thus calculated thickness, refractive index and total porosity parameters are shown in **Table 1**.
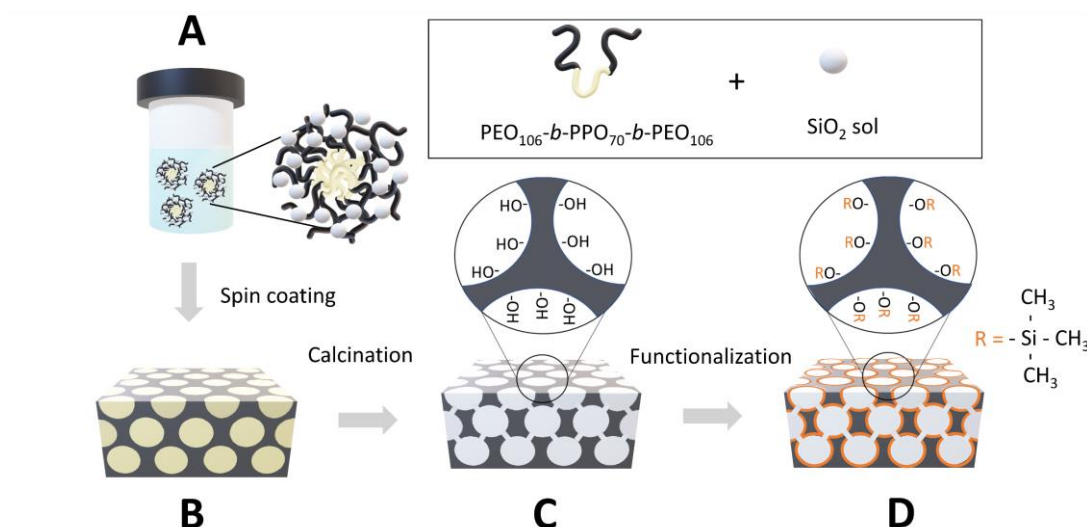

Figure 1. Sol-gel synthesis route towards methyl-functionalized mesoporous silica films. A: polymer-silica hybrid sol, B: polymer-silica hybrid thin film, C: as-calcined mesoporous silica thin film, D: methyl-functionalized mesoporous silica thin film.

To obtain information on the pore structure and to calculate internal contact angles, EP measurements were carried out on the functionalized and non-functionalized silica samples with various adsorptives. The recorded ellipsometric spectra, Ψ and

Δ, of the non-functionalized mesoporous silica films during the pore filling process of a water EP cycle is depicted in **Figure 2**. Tangent of Ψ and Δ denote respectively, the amplitude ratio and the phase difference of the complex reflection coefficients of light polarized parallel and perpendicular to the plane of incidence. As visible, the incorporation of adsorbate molecules caused a spectral shift, which enabled the construction of the volume adsorbed isotherm and PSD calculation using the Lorentz-Lorenz EMA and the modified Kelvin-equation (eq. 1) respectively.

While the capillary condensation range of adsorption isotherms are regularly attributed to size of probed mesopores, desorption behaviors can be an effect of various processes (mainly pore blockage or cavitation [27]), making it less straightforward for internal wetting investigation across different adsorptives. For simplicity, only adsorption isotherms were investigated in this work.

The obtained volume adsorbed isotherms of water on the non-functionalized silica and the series of TMCS-functionalized silica are shown in **Figure 3A**. Analogously, volume adsorbed isotherms were acquired for increasingly non-polar adsorptives (methanol (**Figure 3B**), toluene (**Figure 3C**), and cyclohexane (**Figure 3D**)).

Table 1. Thin film properties of SiO_2 samples functionalized for various times obtained from SE spectra at *P/P$_0$* (water)*=0*.

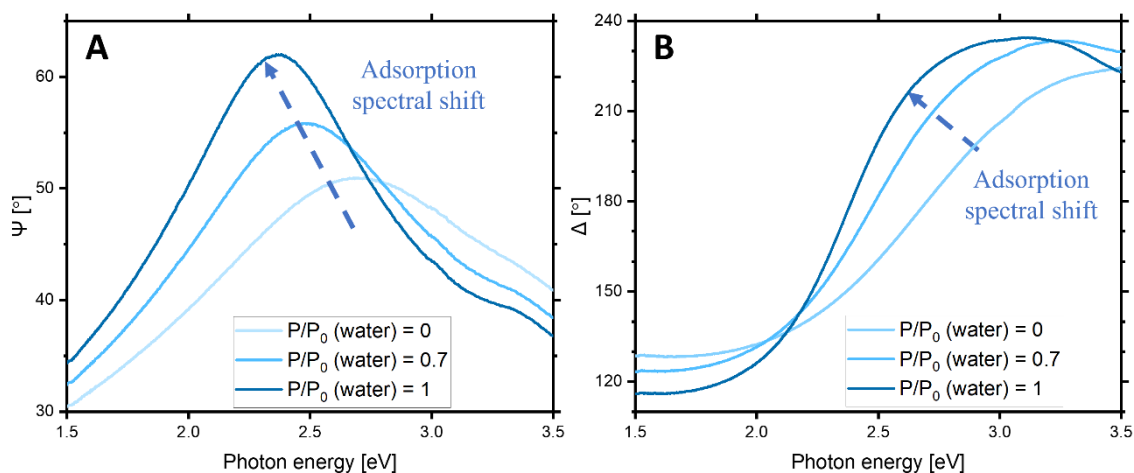| TMCS functionalization time	Thickness (nm)	Refractive index at 632.8 nm (-)	Total porosity (from optical model)
0h	120.1	1.281	35%
30min	102.6	1.272	37%
1h	121.3	1.275	37%
3h	122.6	1.270	37%
5h	120.1	1.272	37%

Figure 2. SE parameters recorded during a water adsorption EP cycle on the non-functionalized silica surface.

As expected, the more hydrophobic functionalized surfaces (30 min, 1 h, 3 h, and 5 h TMCS treatment) obstructed the adsorption of water in the mesopores. The increased number of methyl- and decreased number of hydroxyl-groups present on the surface of the pores delayed capillary condensation, since only the former can undergo strong hydrogen-bond (H-bond) interactions with the adsorbate molecules. Because of the very high surface tension of water, its wetting capability on low-energy surfaces is limited, which explains why the most CH_3-rich surfaces shown on **Figure 3A** (1, 3, and 5 h TMCS treatment) did not reach the saturation adsorbate filling. Using less polar adsorbates (**Figure 3B-D**) we observed similar, but less pronounced effects on delayed capillary condensation. In the case of methanol, this is expected due to the relatively polar nature of the molecule, capable of forming H-bond interactions with the silica surface. In fact, it has been previously reported that even the non-polar benzene and toluene molecules form H-bonds with the hydroxyl groups of silica surfaces via their delocalized π-electrons [28–30], which explains our observations depicted on **Figure 3C**. On the other hand, the completely non-polar cyclohexane exhibits a similar effect (**Figure 3D**), despite the lack of any π-electrons or moieties capable of H-bonding. The underlying mechanism of this phenomenon requires further investigation, which is out of the scope of this paper. Nevertheless, it can be concluded that TMCS-functionalization of silica caused a delay in the capillary condensation of all the tested adsorptives.

Figure 4 exhibits the acquired PSDs for the functionalized surfaces using the 4 tested adsorptives assuming $\theta_i=0°$. Previous authors found the effect of TMCS-functionalization

on pore size to be negligible [31]. Lorentz-Lorenz EMA fitting on the SE spectra of the samples studied in this work confirms this, with all calculated total porosity values falling into the 35±2% range (**Table 1**). This insignificant change in total porosity indicates minimal alteration to the spatial dimensions of the mesopores. Based on this, any deviations in PSDs can be attributed to the incorrect assumption of the internal contact angle, here assumed as of $\theta_i=0°$. The results showcase the severe influence of TMCS-functionalization on the wetting behavior of water and methanol, while results for toluene and cyclohexane were less affected.
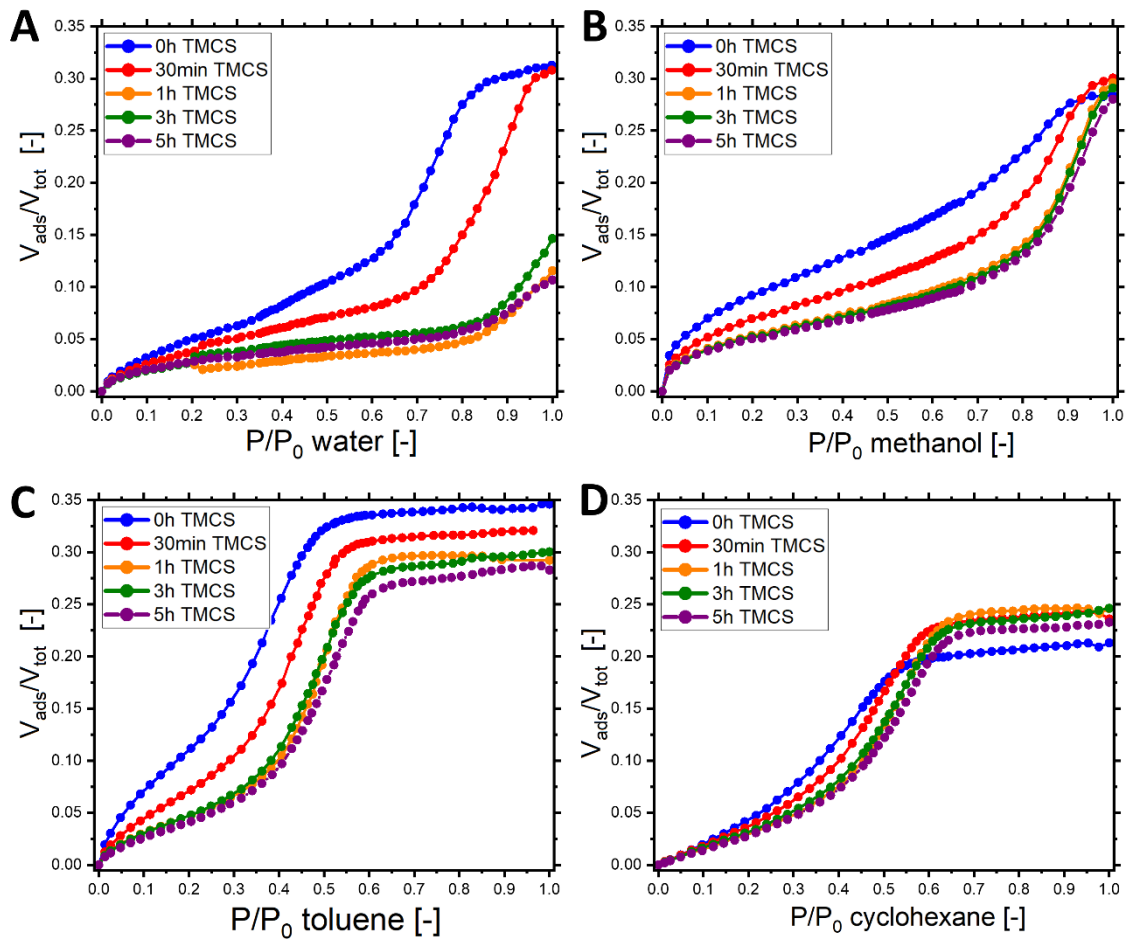

Figure 3. Volume adsorbed isotherms of four different adsorptives (A water, B methanol, C toluene, D cyclohexane) on the series of TMCS-functionalized silica thin films with various treatment times.
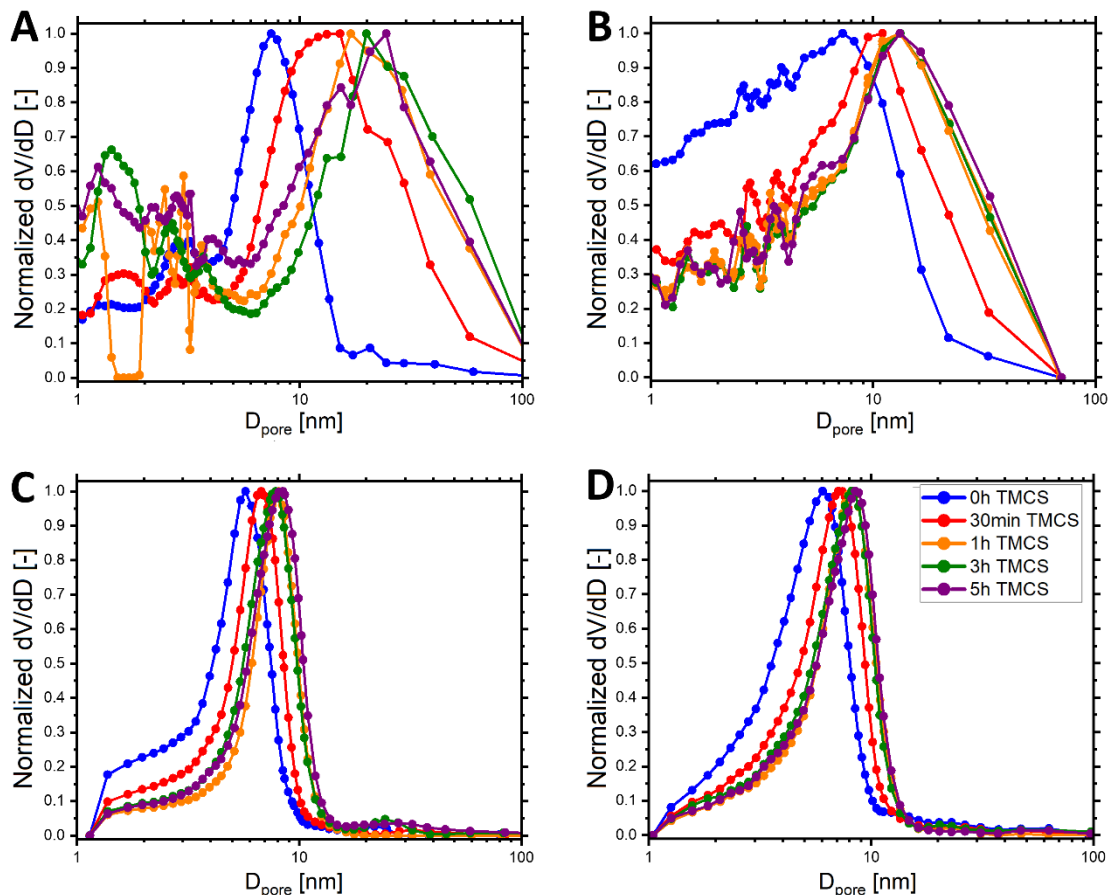
Figure 4. (A-D) Pore size distributions calculated from Figure 3A-D isotherms assuming a 0° internal contact angle for all surfaces.

The PSDs were corrected with modified θ_i values to match the mean pore sizes for the functionalized series (**Figure 5A-D**). The non-functionalized sample was assumed to exhibit 0° internal contact angle towards all four adsorptives to act as reference point for the contact angle fitting of the functionalized surfaces. Since the non-functionalized sample exhibited the earliest capillary condensation within each test of all four adsorptives, and the calculated mean pore sizes are in proximity (6–7 nm), this approximation produces negligible error.

The thus obtained internal contact angles are shown in **Figure 5E** and in **Table 2**. The effect of surface energy as well as the effect of adsorbate polarity can be clearly seen. The apolar toluene and cyclohexane displayed θ_i of around 45–50° after 5 hours of TMCS-functionalization of the silica surface. On the other hand, the increasing polarity of methanol and water resulted in θ_i of over 60° and 70° respectively. It is worth noting that θ_i values obtained for water are lower approximations, as the 1h, 3h and 5h isotherms

clearly did not reach saturation pore filling, meaning that actual θ_i values could be even higher. **Figure 5E** also showcases the effectiveness of evaluating surface functionalization kinetics with EP. θ_i values increased steeply for the first 1 hour of treatment, with smaller changes afterwards. This indicates that the initial (30 min to 1 hour) replacement of the surface hydroxyl with methyl groups corresponds to a larger increase in internal contact angle than the subsequent continued methylation (1h to 5h).
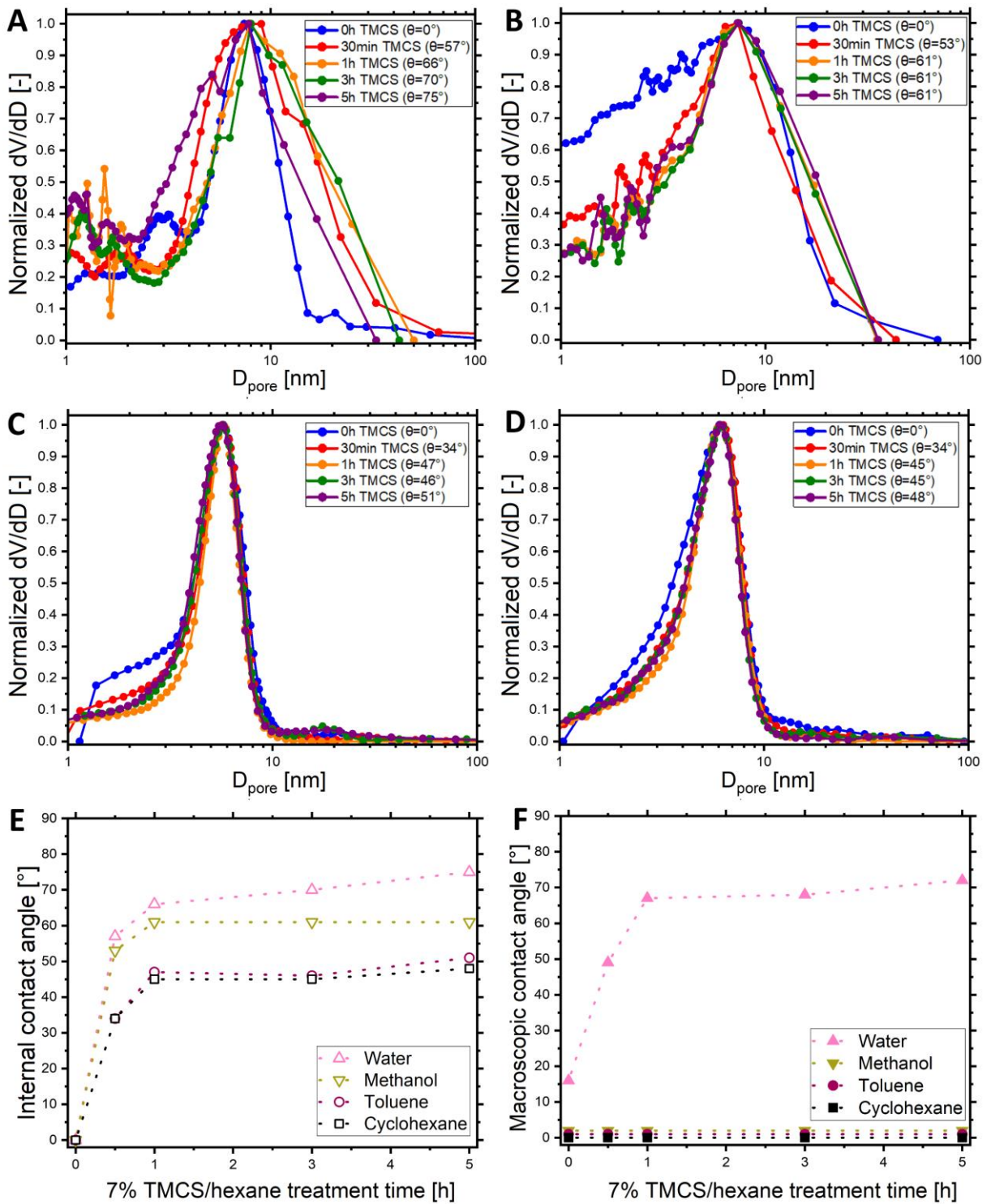
Figure 5. (A-D) Pore size distributions calculated from Figure 3A-D isotherms assuming 0° internal θ for the non-functionalized silica and fitting all other θ_i to obtain matching mean pore sizes. (E) Internal contact angles of the TMCS-functionalized silica surfaces for the four investigated liquids as EP adsorbates. (F) Macroscopic contact angles of the TMCS-functionalized silica surfaces for the same four liquids. All dotted lines are guides for the eye.

XPS was performed to investigate the changes in C, O and Si content and chemical environments with increasing functionalization. Besides the expected Si, C and O peaks, signal related to F was also detected which we relate to sample preparation, where trace contaminants may have been introduced by hexane or TMCS. Full survey spectra is shown in **Figure 6A**. **Figure 6B** shows the C 1s core level spectra where the main peak at 284.8 eV is attributed to adventitious and aliphatic carbon (C^0). Asymmetry to the higher binding energy (BE) side of the main peak (labelled with an asterisk) is due to C-O environments as a result of exposure to air. From analysis of the C 1s core level, a low intensity C-Si environment can be identified on the lower BE side of the main peak in the functionalized samples, which overall increases with TMCS coverage, but this is not easily distinguishable due to the overlap with the main chemical environment. The Si 2p spectra, shown in **Figure 6C,** depict this much clearer with the main Si-O environment and a smaller peak on the lower BE side attributed to a Si-C environments in the functionalized samples (in agreement with the O 1s spectra as shown in **Figure 6D**) [32]. Relative to the Si 2p area, the Si-O peak intensity decreases, and the Si-C intensity increases with increasing functionalization as expected. This was confirmed through peak fit analysis of the Si 2p core level and the resulting ratios of the Si-C and Si-O environments are summarized in **Table 2**. From the Si 2p spectra both the initial appearance of the Si-C environment as well as the clear overall increase of this environment with prolonged functionalization confirm the targeted increasing methyl functionalization of the samples, which is in line with the internal wetting determination experiments. FTIR investigation further validated the XPS observations. In the spectra (**Figure 7**) O-H (3450 cm^{-1}) and C-H (2978 cm^{-1}) stretch bands were identified [33], with a decreasing intensity of the former, and and increasing intensity of the latter with functionalization   time.
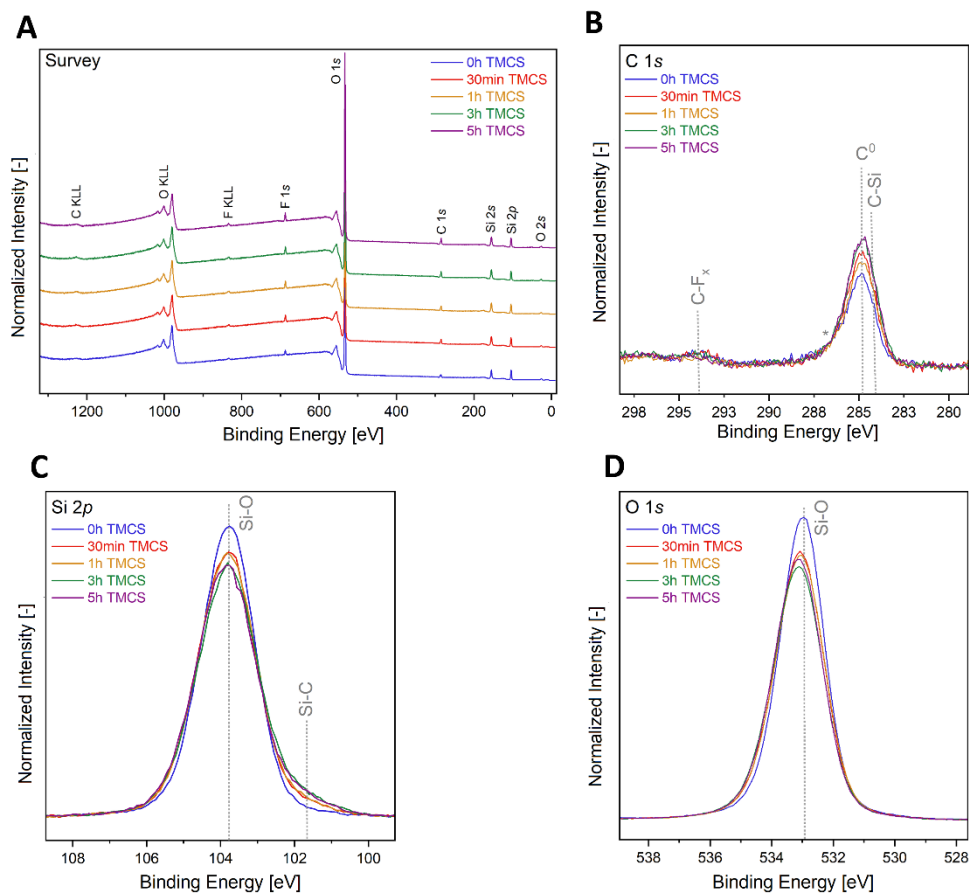
Figure 6. (A) XPS survey spectra collected for the untreated sample and functionalized samples treated with TMCS for increasing amounts of time. XPS core level spectra, including (B) C 1*s*, (C) Si 2*p* and (D) O 1*s*. Core level spectra are normalized to the respective areas of the Si 2p peak to show the change in elemental composition across the samples. The survey spectra are normalized 0-1.
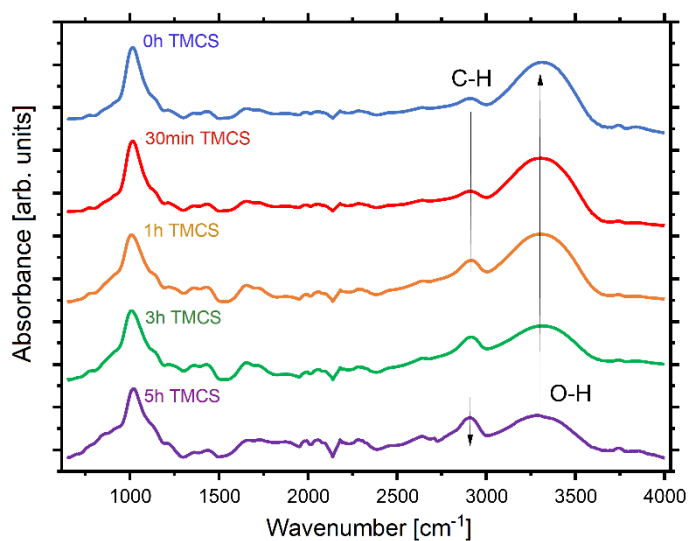

Figure 7. FTIR spectra of the mesoporous silica films after 0h, 30 min, 1h, 3h and 5h

immersion in the 7 vol/vol% TMCS/n-hexane mixture.

To complement the internal wetting and surface chemisty investigations, macroscopic contact angles of the four studied liquids on the functionalized silica films were also studied. Side-by-side comparisons of the changes in both internal and macroscopic contact angles are presented in **Figure 5E-F** and **Table 2**. While in the case of water, a similar trend was observed for both internal and macroscopic wetting, we note that macroscopic contact angles of methanol, toluene and cyclohexane could not be reliably measured due film-like droplet spreading. This indicates near-perfect macroscopic wettability (θ<10°) of the three organic liquids regardless of TMCS-functionalization time. On the other hand, the calculated internal contact angles for these three adsorptives were much higher (θ_i >30°) on the methylated silica surfaces (see **Figure 5E)**. Boudot et al. previously reported significantly higher internal contact values relative to macroscopic ones for alcohol/water liquid mixtures and hydrophobic mesoporous silica [8]. In their work they theorized that due to the heterogeneity of surface chemistry, silanol-rich areas could selectively adsorb the alcohol/water vapors, and that the internal contact angle is more representative of the more hydrophobic parts of the surface. While we observe similar effects with methanol as adsorptive, our findings also show that even non-polar adsorptives (toluene and cyclohexane) exhibit higher internal contact angles compared to their macroscopic ones. This is contrary to the similarity of methylated surface chemistry and adsorptive molecular structure, which highlights the importance of hydroxyl groups for low θ_i values, regardless of adsorptive polarity. These results are further proofs of the inherent differences in the mechanisms between macroscopic and microscopic (internal) wetting.

Table 2. Comparison of internal and macroscopic contact angles observable on the TMCS functionalized silica surface as well as the relative atomic ratio of the Si-C to Si-O environments from peak fit analysis of the XPS Si $2p$ spectra. The estimated experimental error for the latter is ± 0.1 rel. at%.

TMCS treatment time	Internal contact angle (°)				Macroscopic contact angle (°)				Relative Atomic Ratio (%)	
	H_2O	CH_3OH	Tol	C_6H_{12}	H_2O	CH_3OH	Tol	C_6H_{12}	Si-C	Si-O
0h	(0*)	(0*)	(0*)	(0*)	16	<10	<10	<10	0.0	100.0
30min	57	53	34	34	49	<10	<10	<10	1.7	98.3
1h	66**	61	47	45	67	<10	<10	<10	1.8	98.2
3h	70**	61	46	45	68	<10	<10	<10	3.9	98.1
5h	75**	61	51	48	72	<10	<10	<10	4.2	95.8

*Assumed contact angles **Lower approximations

4. Conclusions

In summary, a series of mesoporous silica thin films with increasing methyl-functionalization time were fabricated. The samples were investigated with vacuum ellipsometric porosimetry using a highly polar (water), a moderately polar (methanol) and two highly non-polar (toluene, cyclohexane) liquid as adsorptives. It was found that regardless of adsorptive polarity, methyl-functionalization of the silica surface caused delayed capillary condensation in the obtained volume adsorbed isotherms, although this effect was much more significant in the case of the two more polar adsorptives. The comparison of non-functionalized and functionalized silica surfaces enabled the calculation of internal contact angle values for all four tested liquids. The trends observed in internal θ values highlight the potential of EP as a sensitive tool to monitor surface chemistry modifications based on the change in capillary condensation behavior of methanol, toluene, or cyclohexane.

The experiments and results presented in this work provide guidance for obtaining more accurate pore size distribution via ellipsometric porosimetry. For unknown material chemistries, internal contact angles can be obtained for various adsorptives via employing an identical surface chemistry sample with known pore architecture, geometry, and size as reference. The discussion about internal wetting mechanism can enable and encourage future research in functionalized nanostructured materials and their interfacial behavior with various liquids.

Acknowledgements

References

[1]   B. Reid, A. Taylor, Y. Chen, B. Schmidt-Hansberg, S. Guldin, Robust Operation of Mesoporous Antireflective Coatings under Variable Ambient Conditions, ACS Appl. Mater. Interfaces. 10 (2018) 10315–10321. https://doi.org/10.1021/acsami.7b18299.

[2]   A.J. Kessman, E.E. DeFusco, A.W. Hoover, K.A. Sierros, D.R. Cairns, Sustained Protection for Transparent Electrodes in Touch Panels and Smart Windows: Template Assisted Encapsulation of Fluorinated Silanes in Sol-Gel Silica Films for Sustained Hydrophobic-Oleophobic Functionality, MRS Proc. 1400 (2012) mrsf11-1400-s05-03. https://doi.org/10.1557/opl.2012.91.

[3]   M. Yao, L.D. Tijing, G. Naidu, S.H. Kim, H. Matsuyama, A.G. Fane, H.K. Shon, A review of membrane wettability for the treatment of saline water deploying membrane distillation, Desalination. 479 (2020) 114312. https://doi.org/10.1016/j.desal.2020.114312.

[4]   T. Wagner, S. Haffer, C. Weinberger, D. Klaus, M. Tiemann, Mesoporous materials as gas sensors†, Chem. Soc. Rev. (2013) 4036–4053. https://doi.org/10.1039/c2cs35379b.

[5]   M. Füredi, A. Alvarez-Fernandez, M.J. Fornerod, B. Fodor, S. Guldin, On the rational design of mesoporous silica humidity sensors, (2022). https://doi.org/10.26434/chemrxiv-2022-60dt1.

[6]   Y. He, L. Shao, I. Usman, Y. Hu, A. Pan, S. Liang, H. Xu, A pH-responsive dissociable mesoporous silica-based nanoplatform enabling efficient dual-drug co-delivery and rapid clearance for cancer therapy †, Biomater. Sci. 8 (2020) 3418. https://doi.org/10.1039/d0bm00204f.

[7]   E.A. Franceschini, E. de la Llave, F.J. Williams, G.J.A.A. Soler-Illia, A simple three step method for selective placement of organic groups in mesoporous silica thin films, Mater. Chem. Phys. 169 (2016) 82–88. https://doi.org/10.1016/j.matchemphys.2015.11.033.

[8]   M. Boudot, D.R. Ceratti, M. Faustini, D. Grosso, Alcohol-Assisted Water Condensation and Stabilization into Hydrophobic Mesoporosity, J. Phys. Chem. C. 118 (2014) 23907−23917. https://doi.org/10.1021/jp508372d.

[9]   C. Boissiere, D. Grosso, S. Lepoutre, L. Nicole, A.B. Bruneau, C. Sanchez, Porosity and mechanical properties of mesoporous thin films assessed by environmental ellipsometric porosimetry, Langmuir. 21 (2005) 12362–12371. https://doi.org/10.1021/la050981z.

[10]   P. Löbmann, Characterization of sol–gel thin films by ellipsometric porosimetry, J. Sol-Gel Sci. Technol. 84 (2017) 2–15. https://doi.org/10.1007/S10971-017-4473-1.

[11]   A. Alvarez-Fernandez, B. Reid, M.J. Fornerod, A. Taylor, G. Divitini, S. Guldin, Structural characterization of mesoporous thin film architectures: A tutorial

overview, ACS Appl. Mater. Interfaces. 12 (2020) 5195–5208. https://doi.org/10.1021/acsami.9b17899.

[12] L. Kócs, B. Tegze, E. Albert, C. Major, A. Szalai, B. Fodor, P. Basa, G. Sáfrán, Z. Hórvölgyi, Ammonia-vapour-induced two-layer transformation of mesoporous silica coatings on various substrates, Vacuum. 192 (2021) 110415. https://doi.org/10.1016/j.vacuum.2021.110415.

[13] B. Reid, I. Mane, F. Ahmed, M.J. Fornerod, M. Füredi, B. Schmidt-Hansberg, A. Alvarez-Fernandez, S. Guldin, Enhanced mechanical stability and scratch resistance of mesoporous aluminosilicate thin films, Microporous Mesoporous Mater. 345 (2022) 112246. https://doi.org/10.1016/j.micromeso.2022.112246.

[14] T. Galy, M. Marszewski, S. King, Y. Yan, S.H. Tolbert, L. Pilon, Comparing methods for measuring thickness, refractive index, and porosity of mesoporous thin films, Microporous Mesoporous Mater. 291 (2020) 109677. https://doi.org/10.1016/j.micromeso.2019.109677.

[15] C. Licitra, R. Bouyssou, T. Chevolleau, F. Bertin, Multi-solvent ellipsometric porosimetry analysis of plasma-treated porous SiOCH films, Thin Solid Films. 518 (2010) 5140–5145. https://doi.org/10.1016/j.tsf.2010.03.015.

[16] M.R. Baklanov, K.P. Mogilnikov, V.G. Polovinkin, F.N. Dultsev, Determination of pore size distribution in thin films by ellipsometric porosimetry, J. Vac. Sci. Technol. B Microelectron. Nanom. Struct. 18 (2000) 1385. https://doi.org/10.1116/1.591390.

[17] J. Dendooven, K. Devloo-Casier, E. Levrau, R. Van Hove, S.P. Sree, M.R. Baklanov, J.A. Martens, C. Detavernier, In Situ Monitoring of Atomic Layer Deposition in Nanoporous Thin Films Using Ellipsometric Porosimetry, Langmuir. 28 (2012) 3852–3859. https://doi.org/10.1021/la300045z.

[18] P. Revol, D. Perret, F. Bertin, F. Fusalba, V. Rouessac, A. Chabli, G. Passemard, A. Ayral, Porosimetry Measurements on Low Dielectric Constant—Thin Layers by Coupling Spectroscopic Ellipsometry and Solvent Adsorption-Desorption, J. Porous Mater. 12 (2005) 113–121. https://doi.org/10.1007/s10934-005-6768-9.

[19] M. Bockmeyer, B. Herbig, P. Löbmann, Microstructure of sol-gel derived TiO2 thin films characterized by atmospheric ellipsometric porosimetry, Thin Solid Films. 517 (2009) 1596–1600. https://doi.org/10.1016/j.tsf.2008.09.079.

[20] M. Baklanov, D. O'Dwyer, A.M. Urbanowicz, Q.T. Le, S. Demuynck, E.K. Hong, Moisture Induced Degradation of Porous Low-k Materials, MRS Proc. 914 (2006) 0914-F02-06. https://doi.org/10.1557/proc-0914-f02-06.

[21] A. Khalil, M. Zimmermann, A.K. Bell, U. Kunz, S. Hardt, H. Kleebe, R.W. Stark, P. Stephan, A. Andrieu-Brunsen, Insights into the interplay of wetting and transport in mesoporous silica films, J. Colloid Interface Sci. 560 (2020) 369–378. https://doi.org/10.1016/j.jcis.2019.09.093.

[22] F. Chassagneux, R. Chiriac, F. Bessueille, M. Karabulut, L. Bois, S. Parola, Ellipsoporosimetry and thermoporometry analyses of mesoporous titania film containing silver nanoparticles, Microporous Mesoporous Mater. 139 (2011) 52–58. https://doi.org/10.1016/j.micromeso.2010.10.016.

[23] A. Alvarez-Fernandez, M.J. Fornerod, B. Reid, S. Guldin, Solvent Vapor Annealing for Controlled Pore Expansion of Block Copolymer-Assembled Inorganic Mesoporous Films, Langmuir. 38 (2022) 3297–3304. https://doi.org/10.1021/acs.langmuir.2c00074.

[24] B. Reid, A. Alvarez-Fernandez, B. Schmidt-Hansberg, S. Guldin, Tuning Pore Dimensions of Mesoporous Inorganic Films by Homopolymer Swelling, Langmuir.

35 (2019) 14074−14082. https://doi.org/10.1021/acs.langmuir.9b03059.

[25] D. Zhao, P. Yang, N. Melosh, J. Feng, B.F. Chmelka, G.D. Stucky, Continuous Mesoporous Silica Films with Highly Ordered Large Pore Structures, Adv. Mater. 10 (1998) 1380–1385. https://doi.org/10.1002/(sici)1521-4095(199811)10:16%3C1380::aid-adma1380%3E3.0.co;2-8.

[26] A. Han, Y. Qiao, Effects of surface treatment of MCM-41 on motions of confined liquids, J. Phys. D. Appl. Phys. 40 (2007) 5743–5746. https://doi.org/10.1088/0022-3727/40/18/035.

[27] J. Loizillon, B. Baumgartner, C. Sinturel, M. Abbarchi, B. Lendl, D. Grosso, In-depth study of coating multimodal porosity using ellipsometry porosimetry in desorption scanning mode, J. Phys. Chem. C. 123 (2019) 23464–23479. https://doi.org/10.1021/acs.jpcc.9b05099.

[28] M.S. Nadiye-Tabbiruka, Characterization of the silica surface. I Characterization of modified aerosil by using adsorption of benzene, Colloid Polym. Sci. 281 (2003) 36–44. https://doi.org/10.1007/s00396-002-0741-9.

[29] C. Wang, S.G. Isaacson, Y. Wang, K. Lionti, W. Volksen, T.P. Magbitang, M. Chowdhury, R.D. Priestley, G. Dubois, R.H. Dauskardt, Surface Chemical Functionalization to Achieve Extreme Levels of Molecular Confinement in Hybrid Nanocomposites, Adv. Funct. Mater. 1903132 (2019) 1–9. https://doi.org/10.1002/adfm.201903132.

[30] J. Abelard, A.R. Wilmsmeyer, A.C. Edwards, W.O. Gordon, E.M. Durke, C.J. Karwacki, D. Troya, J.R. Morris, Adsorption of Substituted Benzene Derivatives on Silica: Effects of Electron Withdrawing and Donating Groups, J. Phys. Chem. C. 120 (2016) 13024–13031. https://doi.org/10.1021/acs.jpcc.6b02028.

[31] C. Robertson, A.W. Lodge, P. Basa, M. Carravetta, A.L. Hector, R.J. Kashtiban, J. Sloan, D.C. Smith, Surface modification and porosimetry of vertically aligned hexagonal mesoporous silica films, RSC Adv. (2016) 113432–113441. https://doi.org/10.1039/c6ra23059h.

[32] A. Regoutz, G. Pobegen, T. Aichinger, Interface chemistry and electrical characteristics of 4H-SiC/SiO2 after nitridation in varying atmospheres, J. Mater. Chem. C. 6 (2018) 12079–12085. https://doi.org/10.1039/c8tc02935k.

[33] J. Yang, J. Chen, J. Song, Studies of the surface wettability and hydrothermal stability of methyl-modified silica films by FT-IR and Raman spectra, Vib. Spectrosc. 50 (2009) 178–184. https://doi.org/10.1016/j.vibspec.2008.09.016.